An index for tropical temperate troughs over southern Africa

Satyaban B. Ratna[1*], Swadhin Behera[1,2], J. Venkata Ratnam[1,2], Keiko Takahashi[1,3] and Toshio Yamagata[1]

[1]Application Laboratory, JAMSTEC, Yokohama, Japan
[2]Research Institute for Global change, JAMSTEC, Yokohama, Japan
[3]Earth Simulator Center, JAMSTEC, Yokohama, Japan

*Corresponding Author:

Satyaban Bishoyi Ratna
Application Laboratory, JAMSTEC
Yokohama Institute for Earth Sciences
3173-25 Showa-machi, Kanazawa-ku, Yokohama
Kanagawa, 236-0001 Japan
Email: satyaban@jamstec.go.jp
Tel: +81-45-778-5509
Fax: +81-45-778-5707

Abstract

Strong cases of the tropical temperate troughs (TTT) that are responsible for the most of the summer rainfall over subtropical southern Africa are analyzed. An index for identifying the TTT is introduced for the first time using anomalies of outgoing longwave radiation (OLR) and the wind. The TTT is associated with a ridge-trough-ridge wave-like structure in the lower troposphere over southern Africa and the adjoining Indian Ocean. Therefore, the index considers physical processes that occur over southern Africa, adjoining the Atlantic and Indian Oceans to depict the variability of the TTT events. Unusually strong TTT events are identified when the standard deviations of the TTT indices defined by the OLR and wind anomalies in the selected regions are above 1.5 and 0.5 respectively. After applying this criterion and filtering out consecutive events, 55 TTT events are identified during the study period of December-January-February (DJF) seasons from 1980-1981 to 2009-2010.

From the composite analyses of those 55 events, it is found that the TTTs evolve with suppressed (enhanced) convection over the southwest Indian Ocean adjacent to Madagascar (southern Africa). The suppressed convection is, in turn, found to be associated with the enhanced convection around Sumatra in the southeast tropical Indian Ocean. This may explain why more TTT events occur in La Niña years as compared to El Niño years. Time evolution of the canonical TTT event shows that it starts three days prior to the maturity phase of the event, suggesting possible predictability. After reaching a matured state, the system moves east toward the Indian Ocean and decays within the subsequent couple of days. In addition, the ITCZ structure changes over Southern Africa/Madagascar during the TTT event and remains similar to climatology over other regions. The results indicate that the continental part of the ITCZ intensifies prior to the TTT event and then spreads southward following the mid-latitude influence during and after the event.

Keywords: tropical temperate trough; TTT Index; southern Africa; southwest Indian Ocean; El Niño/La Niña; floods

1. Introduction

Southern Africa (south of 15^0 S) receives most of its rainfall with high spatio-temporal variability during the austral summer (December-January-February, hereafter DJF), except for regions in southwestern South Africa and along the south coast. The dominant rainfall-producing weather system over southern Africa during the austral summer is composed of the synoptic scale tropical temperate troughs (TTTs). The system forms a cloud band and related atmospheric convection that extends along the northwest-southeast direction over both the landmass and the adjacent southwest Indian Ocean (SWIO) region (Harrison 1984; Todd and Washington 1999; Washington and Todd 1999; Todd et al. 2004). The TTTs connect synoptic disturbances in the tropics and mid-latitudes, and can bring heavy rainfall over southern Africa. Cloud band formation is triggered by the arrival of an upper-level trough over southern Africa associated with the band of divergence east of its leading edge. These upper tropospheric troughs play an important role in the development of TTT (Harrison 1984). A significant amount of summer season rainfall and the associated spatio-temporal variability over southern Africa are resulting from the TTT systems. Recent studies suggest that even the interannual variability in the rainfall over southern Africa may be directly related to the variability in frequencies, position and intensity of weather events like TTTs. For example, it has been noted that a quick succession of two events, a 7-day wet spell during 1-7 January 1998, contributed more than 40 % of the 1997/98 November-December-January-February (NDJF) season's rainfall over much of South Africa (Hart et al. 2010).

TTTs are associated with an increase in the intensity of the African Walker cell, with enhanced moisture convergence over tropical southern Africa (Todd et al. 2004) and poleward moisture transport along the cloud bands of TTTs. In a recent study, Hart et al. (2010) suggested that tropical-extratropical interactions over southern Africa may be related to planetary waves. These TTT systems develop over the subcontinent and propagate eastward (Fauchereau et al. 2009). In the maturity stages of TTTs, moisture is transported off the continent along the axis of a band of moisture convergence, rising from near 800 hPa over the landmass into the midlevel flow (700-650 hPa) in the midlatitudes (D'Aberton and Tyson 1996; Todd et al. 2004). The significance of TTTs over southern Africa and SWIO in the transfer of energy and momentum between the tropics and the mid-latitudes were analyzed by Harrison (1984). Although TTTs are the major synoptic rainfall-producing system over South Africa, their physical and dynamical characteristics including the frequencies of occurrence are not well understood.

Some of the earliest studies examined the characteristics of the TTTs using objective methods such as the principal component analysis (PCA) and the cluster analysis (Williams et al. 2007; Washington and Todd 1999; Fauchereau et al. 2009). Williams et al. (2007) conducted PCA to identify the TTT events and suggested that extreme rainfall events are associated with the spatial distribution of TTTs as a result of both local and remote atmospheric and oceanic processes. Washington and Todd (1999) adopted the empirical orthogonal function analysis of satellite-derived daily rainfall estimates to determine the dominant modes of daily summer rainfall variability over southern Africa. Using the cluster analysis of OLR data, Fauchereau et al. (2009) found that maximum convection manifested itself in a northwest/southeast band extending from southern Africa in the subtropics to mid-latitudes of the SWIO (south of 30° S) with the southern ends located between 40° E and 65° E in the Indian Ocean. Considering the importance of the TTTs in the climate of southern Africa, and the complexities in employing the statistical methods used in the above studies, a simple method of identification of the TTTs will contribute to a better understanding of the phenomena not only for seasonal climate forecasting

but also for projection under anthropogenic climate change. Therefore, we formulated an index for TTT, based mainly on the fact that (i) convection exhibits a dipolar structure over southern Africa and eastern Africa/Madagascar, and (ii) there is a ridge-trough-ridge like synoptic pattern extending from the southern Atlantic to the Madagascar region. The index created with these criteria is discussed in detail in section 4. The observed features of the TTTs identified by using the present index are discussed in sections 5 and 6.

2. Data

Daily data for the DJF season from 1980-1981 to 2009-2010 (30 year) was used to create the TTT index. A set of the daily mean data of sea level pressure, geopotential height, vertical velocity omega, specific humidity and the zonal and meridional winds from the National Centers for Environmental Prediction/National Center for Atmospheric Research (NCEP/NCAR) reanalysis (Kalnay et al. 1996) was used. We selected the data after 1980 since the quality has improved because of the availability of better and more reliable data from satellite and in situ observations, particularly for the NCEP/NCAR reanalysis data set over the Southern Hemisphere [e.g. Kistler et al. (2001) and Trenberth et al. (2001)]. The National Oceanic and Atmospheric Administration (NOAA) interpolated outgoing longwave radiation (OLR; Liebmann and Smith 1996) was also used as a proxy to the observed rainfall. OLR data have been used in several other studies of the TTT phenomenon (e.g. Fauchereau et al. 2009; Pohl et al. 2009). In addition, the NOAA optimum interpolation (OI) daily sea surface temperature (SST) V2 (Reynolds et al. 2007) available at 0.25 degree resolution was used to analyze the impact of the oceans on the TTTs. The daily anomalies were created from the daily mean from 1980-1981 to 2009-2010. To study the El Niño - Southern Oscillation (ENSO) and TTT relationship, we used the global precipitation climatology project (GPCP) monthly mean rainfall (Adler et al., 2003) and monthly mean NOAA OI SST, NCEP/NCAR reanalysis winds and geopotential height data for the DJF season.

3. December-February Climatology over the Study Region

In this section we show the seasonal climatology of southern Africa, which helps us in understanding the background state prior to the formation of TTT events. Southern Africa, owing to its subtropical location, is influenced by weather systems from both low-latitudes and mid-latitudes. The region experiences semi-arid conditions and except for the southwestern part of the Western Cape Province of South Africa, it receives most of its rainfall in austral summer. The southern coast of South Africa receives rainfall throughout the year whereas the western interior experiences rainfall mainly during late summer/autumn. As shown in Fig. 1a, seasonal rainfall in the northern part of southern Africa and Madagascar are associated with the southernmost position of the Inter-Tropical Convergence Zone (ITCZ).

It can be noted that there are two semi-permanent subtropical high pressure regions (Fig. 1b), one over the Atlantic Ocean (known as the St. Helena High or the South Atlantic High, SAH) and the other over the Indian Ocean (known as the Mascarene High, MH). The eastward ridging of SAH often induces onshore flow that causes rainfall along the southern coast and sometimes up to the eastern coast. Sometimes the rain band extends in the northwest direction and couples with surface depression in the Mozambique Channel. This produces an easterly wave flow into Mozambique and eastern South Africa. Continental heat lows associated with weak cyclonic circulation (Racz and Smith 1999) often form over the central Kalahari (Fig. 1b).

The climatology of winds and geopotential height at 850 hPa (Fig. 1c) and 500 hPa (Fig. 1d) shows lower and middle tropospheric circulation over southern Africa. The winds converge from the equatorial region and the easterlies arrive from the SWIO and westerlies from the southern Atlantic. The convergence of these major airstreams induces vertical motion, and thus tropical lows and troughs tend to form in these convergence zones. The Angola low is a semi-permanent feature of the southern African circulation during summer (Fig. 1c) and it dominates the circulation from the low-level to mid-level troposphere (Reason et al. 2006). Besides the Angola Low, the other formation sources/mechanisms for TTTs are recognized particularly in response to both the topography (Bie Plateau) as well as lower tropospheric heating. Also, heat lows can form over Botswana or Mozambique. There are also troughs that form in the Mozambique Channel or over eastern Madagascar that can act as TTT source regions. The circulation at 500 hPa (Fig. 1d) shows the presence of an anticyclonic circulation centered over Namibia and Botswana during this season known as the Botswana High.

The divergence and the vertical velocity at 850 hPa and 500 hPa are shown in Figure 1e and 1f respectively. There is a zone of convergence (Fig. 1e) in the western part of southern Africa extending from the Angola Low (15^0S) to South Africa (32^0S). This convergence zone is associated with upward motion. Adjacent to the west of this convergence zone, there is a divergence zone on the eastern border of the Atlantic Ocean associated with the subsidence. The divergence and convergence zone over the eastern Atlantic Ocean and southern Africa comprises a dipole structure. This dipole pattern is reversed at 500 hPa. There is an upward (downward) motion at this level associated with convergence (divergence) region. The representation of the system at this level also shows a dipole structure. The 850 hPa and 500 hPa level features remain opposite to each other and represent the baroclinic structure of the atmosphere. The weakening and strengthening of the mid-level anticyclonic circulation or the Botswana High influence the spatial distribution of rainfall over southern Africa (SADC, 2001)

4. Tropical Temperate Trough Index

Previous studies have shown that the TTTs cause enhanced (suppressed) convection over southern Africa (eastern Africa/Madagascar) (Washington and Todd 1999; Fauchereau et al. 2009). Also it was found earlier that the TTTs are accompanied by baroclinic ridge-trough-ridge wave-like structure in the lower troposphere over southern Africa and the surrounding Atlantic and Indian Oceans. It was observed that there are three possible locations of TTT over the regions extending from southern African mainland to Madagascar (Fauchereau et al. 2009; Pohl et al. 2009 and Vigaud et al. 2012). Some of the TTT events are known to occur over the southern African mainland and have a tendency to propagate eastward toward the Mozambique Channel and Madagascar. The extreme rainfall associated with strong TTT events generally causes flooding over southern Africa, which is the westernmost part of the above mentioned TTT region. When TTTs move or form east of the mainland, much of the rain falls over the ocean and hence does not affect society directly. In view of this we defined an index for identifying the TTTs over the southern African mainland.

In order to define indices for the TTT activities, we examined the reanalysis data over the key regions such as the southeast Atlantic Ocean, southern Africa and eastern Africa/Madagascar. Taking into account the critical role of atmospheric convection in TTTs, we used the OLR anomalies averaged over the regions (W1, W2, E1, and E2) shown in Fig. 2 to form the index. This is because of the existence of negative/positive OLR anomalies over these regions. Generally, negative OLR anomalies are elongated from southern Africa to

southwest Indian Ocean, and the positive OLR anomalies are elongated from eastern Africa to the Madagascar region. Similarly, a ridge-trough-ridge structure of the system occurs over the Atlantic Ocean, southern Africa and SWIO. Since this is the basis of the TTT formation, we have also incorporated the meridional component of wind averaged over the regions (W and E) shown in Fig. 2 as the other atmospheric parameter defining the index. The wind component of the index determines the horizontal wind shear and is defined as the difference between the meridional wind anomalies of southeast Atlantic Ocean and those of the southwest Indian Ocean ($V850_{SEAO} - V850_{SWIO}$). All the previous studies identifying the TTTs are based on OLR but our study is different as we have added another variable, 850 hPa winds for the robustness of the index.

We prepared the daily anomalies for DJF from the 30 years (1980/1981 – 2009/2010) climatology to formulate the TTT Index. Because of the unique dipolar nature of OLR and the wave structure of wind anomaly as discussed above, each index is composed as follows:

$$OLR = ((OLR_{E1}+OLR_{E2})/2.0)*0.4) - ((OLR_{W1}+OLR_{W2})/2.0)*0.6) \quad \text{---------- (1)}$$

$$Wind = V_W - V_E \quad \text{---------- (2)}$$

We define a TTT event with the condition that the standard deviations of OLR and wind exceed 1.5 and 0.5 respectively. The 1 standard deviation values for OLR (Eq. 1) and wind (Eq. 2) are 16.37 and 4.99 respectively. The subscript in equation (1) represents the area averaged OLR anomaly over each of the regions, E1 (37^0E – 42^0E, 17^0S – 12^0S), E2 (45^0E – 50^0E, 23^0S – 15^0S), W1 (22^0E – 32^0E, 24^0S – 18^0S), and W2 (32^0E – 42^0E, 36^0S – 28^0S), respectively (Fig. 2). These four boxes are picked for OLR due to the dipolar structure of convection orientated in the northwest-southeast direction in the case of TTT events. The values 0.4 and 0.6 in equation (1) are the weighting factors for the eastern and western regions respectively. These values are chosen as per the regional strength of anomalies between the east and west regions. We find that the anomalies in the western region are stronger than those in the eastern region. Thus, we have given more weighting to the western region (0.6) compared to the eastern region (0.4) after testing these parameters with varying intensity. Similarly, the subscript in equation (2) represents the area averaged meridional wind anomaly over each of the regions W (0^0E – 15^0E, 38^0S – 27^0S) and E (34^0E – 46^0E, 38^0S – 27^0S), respectively (Fig. 2). We arranged all these boxes in such a way that the TTT over southern Africa identified by our index matches those found in earlier studies (Fauchereau et al. 2009, Pohl et al. 2009) and these are the best possible choices to identify the TTT systems. This index is useful in such a way that we can identify the TTT for a particular day from the available OLR and wind data.

Based on the criterion mentioned above, we found 91 days of the TTT event from 30 years of data when both conditions are satisfied. It is also seen that by changing the standard deviation of OLR to 1.0 and by keeping the same value of 0.5 for the standard deviation of wind, we obtained 198 events. The corresponding composite maps for the 91 events and 198 events are presented in Fig 2b and Fig 2c respectively. It is found from those composite maps that the dipolar structure of the convection for the 91 events was stronger than that for the 198 events. Since this study focuses on intense TTT events, we considered the 91 strong TTT events for further analysis. However, several consecutive days of events [some of the events have persisted for 3-4 days as reported by Todd and Washington (1999) and Vigaud et al. 2012] found in this method make it difficult to form

the basis for the lead-lag analysis in the composite study. So, we filtered some of those days by retaining the days of maximum OLR anomaly as the intense TTT events. After filtering out those days, we have retained 55 events for further analyses.

The monthly distribution of TTT events indicates a higher number of occurrences in December (22 events), followed by January (17 events) and February (16 events). The average annual frequency of the extreme TTT event is 1.83 during the 30 years (Fig 3) of the study period. Figure 3 indicates that the frequency of the event is less during the decade 1980-1989. There are no TTT events during the austral summer season of 1982-83, 1983-84 and 1986-87. A maximum of 3 events during the 1980s have seen in the years 1980-81 and 1987-88, which coincide with La Niña events in the Pacific. During the 1990s, almost all year except for the austral summer seasons of 1991-92 and 1996-97 are associated with the events. During the period 1998-2009, the TTT event is observed every year. In particular, four events per season are seen in 1998-99, 2000-01, 2003-04, and 2008-09. Overall, there are 14 events during the decade 1980-89, 18 events during 1990-99 and 23 events during the decade 2000-2009.

The standardized anomalies of OLR and winds for the above 55 events are presented in Fig. 4. In the decade of 1980-1989, except for one event during 1988-89, no TTT events are observed during the DJF season in 1982-83, 1983-84, and 1986-87. Out of these four seasons, 1982-1983 and 1986-1987 are El Niño years. Three TTT events occurred during the period December 1987 - January 1988 with only a few days gap. This exception might be related to the 1987-88 La Niña. The interannual variability in the number of occurrences is shown to be modulated by distinctive seasonal SST anomaly patterns, which make it possible to focus on the interactions in the interannual time-scales. A substantial part of interannual rainfall variability over the region is known to be directly linked to changes in the frequency of TTTs (Todd and Washington 1999). At interannual time scales, southern Africa rainfall variability has been linked to El Niño/Southern Oscillation (ENSO) in earlier studies (e.g. Richard et al. 2000). Though the average atmospheric convection is weaker during El Niño years, subseasonal fluctuations in the OLR tend to be larger during these years (Vigaud et al. 2012).

In the decade of 1990-1999, there are no TTT events observed during the El Niño season 1991-92 and only one event during the El Niño of 1997-98. In the other El Niño year of 1994-95, only two TTT events have developed. On the other hand, 2, 4 and 3 TTT events evolved during the La Niña years of 1995-96, 1998-99 and 1999-00, respectively. In the decade of 2000-2009, only the El Niño years of 2002-03 and 2004-05 had one TTT event and all other years in this decade are associated with more than one TTT event. The annual frequency of TTTs in DJF correlates well with the Nino3.4 index with a value of -0.44, which is statistically significant at the 95 % level using the student's t-test.

During the study period, 11 TTT events appeared in 10 El Niño years (average 1.1) whereas 18 TTT events appeared during 7 La Niña years (average 2.6). Since the annual frequency of the intense TTT events is 1.8, it is therefore evident that TTT events are associated more with La Niña than El Niño year. The impacts of the ENSO on the climate of the surrounding subtropical region may be attributed to the Rossby wave train generated by the diabatic heating in the tropical Pacific. The Hadley circulation due to the tropical forcing also induces changes in convergence/divergence patterns in the subtropics that in turn act as a Rossby wave (Trenberth et al. 1998) source, subject to some constraints such as the location of heat source and interaction with the climatological stationary planetary waves. The atmospheric response to the El Niño is baroclinic in the tropics, whereas it has an equivalent barotropic structure in the subtropics. The basic mean state of

midlatitudinal atmospheric circulation plays an important role in transmitting the energy from the tropics to midlatitudes (Hoskins and Karoly, 1981; Trenberth et al., 1998; Diaz et al., 2001; Kidson et al., 2002). The TTT and an associated favorable teleconnection are further discussed in section 7.

5. Temporal evolution of TTTs

In the following section the temporal evolution of the TTT event is described. All the description is based on composite pictures derived using atmospheric fields from several days before to two days after the event. For easier understanding, we have divided the evolution of the event into three stages: (i) developing stage - from several days to one day prior to the event, (ii) mature stage – the day of the event, and (iii) decaying stage – two days after the event.

5.1 Developing stage

To understand the mechanism of the TTT formation, we have analyzed the global distribution of OLR from day -7 to day -4 prior to the event (Fig. 5). A region of significant positive OLR is seen near Madagascar on day -7, and this persists till the maturity stage of the event. On the other hand, a region of negative OLR is observed over the Sumatra region during the same period, corresponding to the positive SST anomalies in the region. From day -7, a negative OLR region is present over the tip of southern Africa and parts of northern Africa. The region of negative OLR intensifies over southern Africa from day -4 and persists until the TTT event attains its maturity.

To study the cause of the positive OLR anomalies near Madagascar, we have plotted the velocity potential anomalies at 200 hPa from day -7 to day -4 (Fig. 6). From the figure one can clearly see a region of upper level convergence in the western Indian Ocean near Africa and Madagascar. On day -7 and day -6, the convergence is mainly due to the accumulation of air mass which diverges from Indonesia and northern Africa. This pattern appears to be related to the changes in the Walker circulation during the La Niña condition in the Pacific as seen in SST anomalies (Fig. 8). The higher level convergence near Madagascar draws upper-tropospheric flow from the southern Africa landmass on day -6 and this generates divergence over the landmass. This upper-level divergence over the landmass during day -6 and day -5 (Fig. 6) causes vertical uplifting and this may induce anomalous low-level convergence (Fig. 7) over southern Africa. On day -4, an upper level divergence over the southern Africa and low level convergence over the Angola region are seen, indicating an intensification of the related convection, which is clearly reflected in the OLR anomaly (Fig. 5). Therefore, we assume that the formation of TTTs is mainly favored with the enhanced tropospheric convection in the Sumatra region during the La Niña conditions in the Pacific. The La Niña conditions seem to modify the Walker circulation, with upper level convergence over the equatorial Indian Ocean near the African continent and Madagascar region.

Figure 9 depicts the development stage of TTTs by use of the composite anomalies of OLR and 850 hPa winds from three days before (day -3) to two days (day 2) after the event. A cloud band indicating anomalous enhanced convection appears over Angola, Namibia and Botswana on day -3. At this time, anomalous easterly winds at 850 hPa are found to enter eastern Africa from the southwest Indian Ocean, north of Madagascar. Also, we find suppression of atmospheric convection in the maritime regions. On the following day (day -2), the negative OLR anomalies are further strengthened and extended toward south and east over the

continent. At this time, a region of enhanced convection is seen over southern Africa. Also, a mid-latitude transient system approaches with a weak trough over southern Africa and a ridge over the southern Atlantic Ocean. In contrast, atmospheric convection continues to be suppressed off eastern Africa and the anomalous dry zone extends across eastern Africa and Madagascar.

On day -1, the anomalous low-level winds are strengthened from the SWIO and the tropical region. The mid-latitude transient over southern Africa also intensifies over the southern South Atlantic. The OLR anomalies show a dipole structure with more rain over southern Africa and less rainfall over the Madagascar region. The composite of the sea level pressure anomalies (Fig. 10) shows that, on day -2, a significant high pressure is seen over Madagascar and the adjoining SWIO, linking the convection over Sumatra with subsidence over this region discussed earlier. Another high pressure system is seen over the South Atlantic, eventually resembling the ridge-trough-ridge structure found in the earlier studies (Todd et al. 2004). The trough between the ridges becomes more prominent on day -1. As seen in Fig. 11, the evolution of the vertical velocity anomalies is in agreement with that of the sea level pressure. On day-3, subsidence occurs over the eastern Africa, Madagascar and the adjacent Indian Ocean and vertical uplift develops over South Africa on day-1.

5.2 Mature stage

On day 0 the cloud band is further strengthened before reaching the full maturity state (Fig. 9). The anomalous cloud band elongated in the northwest-southeast direction and the associated trough extends from 15^0S on the African continent to 45^0S on the southwest Indian Ocean. At the same time, convection is suppressed over eastern Africa and Madagascar and the associated ridge extend from northwest to southeast in the Indian Ocean (Fig. 9). The suppressed convection extending from 10^0S in eastern Africa to 35^0S in the southwest Indian Ocean is composed of a dipolar structure with enhanced convection associated with the elongated trough. The structure and orientation of the TTT cloud band is similar to the finding of earlier studies (e.g. Washington and Todd 1999, Fauchereau et al. 2009, Pohl et al. 2009, Vigaud et al. 2012). The anomalous cloud band is located above a lower level anomalous trough that extends from the tropics to the midlatitudes. This, in turn, is associated with an anomalous ridge-trough-ridge structure across the region. There is a cyclonic circulation located over southern Africa while anticyclonic circulations prevail to the west and east of it. Strong winds are found along the trough over southern Africa as reported in earlier studies (D'Abreton and Tyson 1995; Todd et al. 2004) in addition to the westerly flow from the Atlantic (D' Abreton and Tyson 1995; Cook et al. 2004, Hermes and Reason 2009; Vigaud et al. 2009). These two flows converge over southern Africa and contribute to summer rainfall (Reason 1998) and then move southward along the axis of TTT. This system represents an important mechanism of the poleward transport of energy and momentum. There is also a ridge structure over Madagascar/southwest Indian Ocean but this is less intense than that over the Atlantic Ocean.

At the maturity stage of the TTT event, the sea level pressure distribution shows an enhanced anticyclonic circulation over the Indian Ocean centered over 30^0S and 50^0E extending northwestward into Madagascar (Fig. 10). This high is associated with the anticyclonic circulation over the Indian Ocean and helps to bring moisture from the Indian Ocean to the east coast of Africa. The genesis of the TTT event is associated with the strengthening of these easterly winds. The anomalous sea level pressure further indicates that a trough extends from the tropics to midlatitudes and the cloud band coincides with this anomalous trough. It is also evident from the vertical velocity at 850 hPa (Fig. 11) that there is upward motion in the lower atmosphere that

extends up to 200 hPa. The vertical uplift over South Africa reaches its maximum on day 0. These strong vertical motions are associated with low level convergence and strong upper level divergence (not shown). Earlier studies have suggested that the strong vertical velocity is related to TTT and deep convection (van den Heever, 1997; Dyson and van Heerden, 2002; Hart et al. 2010). Surface convection and upper air divergence result in ideal conditions for strong vertical uplift and the formation of cloud bands across the subcontinent to the southwest Indian Ocean. It is known that the TTT events are influenced by the position of a semi-permanent surface-low known as the Angola Low, located over southern Africa. A cloud band usually forms over southern Africa when the low is situated over the Namibia-Angola region (Harrison 1984). In such a situation, low level easterlies are likely to prevail over subtropical southern Africa, drawing moisture from the southwest Indian Ocean. At the same time, anomalous westerlies to the north of the surface low carry moisture from the tropical South Atlantic Ocean.

Previous studies have shown that moisture is transported to the midlatitudes along the TTT axis (D'Aberton and Tyson 1995; Todd et al 2004). To understand this process, we have defined the moisture transport vector as $\mathbf{Q} = q\mathbf{V}$. The total wind vector $\mathbf{V}$ is composed of the zonal and meridional winds and q is specific humidity. The use of the Helmholtz theorem allows us to separately describe the moisture transport ($\mathbf{Q}_\psi$, rotational) and flux divergence ($\mathbf{Q}_\chi$, irrotational) as $\mathbf{Q} = \mathbf{Q}_\psi + \mathbf{Q}_\chi$ (e.g., Behera et al. 1999; Todd et al. 2004). Here, ψ denotes streamfunction and χ denotes velocity potential.

The composite of the rotational part of the moisture transport anomalies (Fig. 12) shows the formation of a cyclonic circulation over South Africa and the adjacent Indian Ocean during the genesis of the TTT event. During the formation of the event, the seasonal mean anticyclonic circulation weakens over the eastern parts of southern Africa including the Mozambique Channel and a pronounced anomalous cyclonic flow develops. This cyclonic flow gradually intensifies from day -1 to the day 0, and then reduces to negligible intensity. The anticyclonic circulation to the east of the TTT evolves as part of the ridge of the mid-latitude circulation. During the days after the maturity stage, only the oceanic region receives the maximum moisture flux; the region moves further eastward in the following days.

The composite anomalies of moisture transport (divergent) at 850 hPa are presented in Fig. 13. The velocity potential associated with divergent moisture flux variations shows a north-south dipole structure and reaches its maximum at the maturity stage (day 0). The maximum (minimum) velocity potential in the figure corresponds to the region of convergence (divergence). The maximum divergence zone lies in the northern parts of southern Africa at around 20^0S. Similarly, the maximum convergence zone is centered at 40^0S and 40^0E. During this maturity stage, divergence is dominant over land and convergence over the oceans. The high moisture flux in the TTT band is maintained by a divergent flux largely from the southwest Indian Ocean near Madagascar. The divergent flux seems to be linked to the above normal convection in the Sumatra region and the associated subsidence over the southwest Indian Ocean as mentioned earlier. In the region of study, the rotational part is larger than the potential part and the total moisture flux is well represented by the former (Chen 1985). In particular, along the TTT axis, rotational winds exceed winds associated with the velocity potential, in agreement with the study by Todd et al. (2004).

5.3 Decaying stage

After Day 0, the TTT event starts decaying with the eastward passage of the anomalous cyclonic circulation (Fig. 9). Consequently, the ridge-trough-ridge structure also becomes less intense though strong flows still remain along the cloud band. Sea level pressure anomalies indicate that, on day +1, all three components, namely the trough, Mascarene High and SAH, lose their intensities (Fig. 10). The SAH moves northeastward to southern Africa and pushes the trough further eastward. On day +2, the cloud band moves further eastward and continues to reduce in intensity (Fig. 9). The western edge of the trough at 35^0S is located at 30^0E during the TTT event. On day +1, it moves eastward to 35^0E and, on day +2, it moves further eastward to 40^0E along the same latitude of 35^0S. This eastward movement of the TTT found in our study is consistent with some of the previous studies (e.g. Fauchereau et al. 2009). The intensity of convection also further reduces after day +2 and no significant sea level pressure anomaly is found. The strength of subsidence over Madagascar also weakens in the two days (day +2) following the event.

6. TTT and global circulation

The large scale patterns of the circulations in southern midlatitudes are analyzed to understand the association of planetary waves with the genesis of TTT event. From the 200 hPa meridional wind composites (Fig. 14), we find propagation of the mid-latitude transients to southern Africa during the initiation and maturity stages of the TTT event. From day -3 to the maturity stage, the trough-ridge-trough pattern of the eddy is seen at 200 hPa extending from the southern Atlantic to Madagascar. The OLR distribution from day -3 to day +2 is presented in Fig. 15. One prominent feature of the global OLR distribution is that the TTT is the only significant disturbance during the development of the TTT event. However, prior to the genesis (Fig. 6), we notice above normal convection over the maritime regions near Sumatra. The diabatic heating anomalies associated with the convection could project onto the mid-latitude waveguide to help the transients move from the southern Pacific Ocean to southern Africa. In addition, the ITCZ structure changes over Southern Africa/Madagascar during the TTT event and remains similar to climatology over other regions (Fig. 15). It seems that the ITCZ does not change its position but breaks down during the TTT. The ITCZ intensifies prior to the event and then spreads out south following the mid-latitude influence during and after the event.

The composite anomalies of sea surface temperature (Fig. 8) indicates that anomalously warm sea surface temperatures are observed over the Mozambique Channel, southwest Indian Ocean and the South Atlantic Ocean. These patterns are apparently associated with the co-evolving subtropical SST dipoles in the south Indian and south Atlantic Oceans but the positive anomalies appear to be more significant (Manhique et al 2011). The anomalies in the South Atlantic Ocean are far from the coast compared to the anomalies in the Indian Ocean. Therefore, the main source of moisture for TTT development is the Indian Ocean as the easterly winds enter the continent from the warm oceanic region adjacent to the continent. As the sea surface temperature is high over this region, low-level air above the ocean contains more moisture. The easterly flow over this region helps to transport this moisture from the Indian Ocean to the southern African continent. The link between the warm anomalies of SST over SWIO with positive anomalies of rainfall over southeastern Africa was reported by Reason and Mulenga (1999). Behera et al. (2000), Behera and Yamagata (2001), Reason (2001) and Washington and Preston (2006) extended this and explained that the SST dipole phenomenon with warm SST anomalies in the southwest and cool SST anomalies in the southeast in the southern Indian Ocean is

related to an increase in rainfall over southeastern Africa. Also, Williams et al. (2007) reported that the region of warm oceanic surface temperature anomalies has an indirect effect on rainfall variability by suppressing the Walker cell, enhancing the Hadley-type circulation and low pressure over equatorial southern Africa.

7. TTT and ENSO

This study indicates that the La Niña events are associated with more number of TTT events as compared to that of El Niño events. To understand the mechanism and background climate state further, we have used December-February composite anomalies of 5 El Niño, which also included Indian Ocean Dipole years (Saji et al. 1999; Yamagata et al. 2004; Behera et al. 2005) and 7 La Niña events which occurred during the study period of 30 years. The southern Africa rainfall association with ENSO is already discussed in many previous studies. Here, we have tried to provide the background climate characteristics that could be attributed to TTT evolution.

During the El Niño events the Walker circulation changes owing to rising and sinking motions associated with higher than normal rainfall over the central and equatorial eastern Pacific and less than normal rainfall over the western Pacific, Maritime Continent and the Indonesian Sea (Fig. 16a). These rainfall anomaly patterns are associated with warm (cool) sea surface temperature anomalies over the eastern (western) Pacific (Fig. 16c). The changes in diabatic heating during El Niño cause upper level divergence (convergence) over the eastern (western) Pacific (Fig. 16e). The anomalous rainfall, sea surface temperature and velocity potential patterns are opposite during the La Niña seasons (Fig. 16b, d).

The modification of the Walker circulation across the Pacific can induce changes in the atmospheric circulation over the adjacent Indian and Atlantic Ocean basins as well. Associated with the anomalous Walker circulation and to some extent with the anomalous Rossby waves discussed in the next paragraph, we find an anomalous upper level (lower level) convergence (divergence) over southern Africa during El Niño events (Fig. 16a). The anomalous lower level divergence over the landmass prevents maritime moisture transport to southern Africa, thereby reducing the seasonal rainfall (Fig. 16a). Since moisture feed from the southwestern Indian Ocean plays a major role in the TTT formation, the El Niño related background condition does not favor the TTT genesis. The situation becomes opposite during La Niña season when anomalous upper level divergence (lower level convergence) over southern Africa (Fig. 16d) enhances the continental rainfall (Fig. 16b) in that region. The anomalous convergence of moisture to the landmass favors the genesis of TTTs. This is confirmed from the composite anomalies of 55 TTT events described in the temporal evolution of the events in Section 5.1.

In addition to the tropical connections, we find that ENSO could influence the TTT genesis through the extratropical teleconnections of the Southern Hemisphere waveguide. The midlatitude regions of the Southern Hemisphere are known for planetary waves of wave-number 3-6 due to atmospheric instability. From the composite anomalies of upper level meridional winds (Fig. 16 e, f) we find wave number 6 type of teleconnection arising from ENSO. The paths of the waves are similar to the preferred propagation paths for Rossby waves in these regions (Hsu and Lin 1992; Hoskins and Ambrizzi 1993; Cook, 2001).

The equivalent-barotropic response to the mid-latitudes waves, associated with La Niña, is an anomalous high just south of South Africa (Fig. 16f). This anomalous anticyclone will favor mid-latitude winds flow towards continental southern Africa and hence favor TTT genesis. We saw earlier that the TTT forms as a ridge-trough-ridge structure over this region due to interaction between midlatitude and tropical disturbances.

The circulation anomaly is opposite during the El Niño season (Fig. 16e) when we observe an anomalous low in the midlatitude region south of South Africa discouraging the tropical-temperate interactions.

8. Summary

It is well established that the TTT is the main rainfall producing synoptic system over subtropical southern Africa and the southwest Indian Ocean, and it represents an important mechanism of poleward transport of energy, moisture and momentum (Todd and Washington 1999; Washington and Todd 1999; Todd et al 2004). So far, various analysis methods like cluster analysis and PCA have been adopted to study the TTT objectively. However, those methods were not able to describe the TTT in a simple way from the observational data. This study is novel in the sense that a TTT index has been newly introduced based on the daily OLR and wind data obtained from the NCEP reanalysis product. Because of its simple formulation using easily available observed data, the index provides an excellent opportunity to identify and study the TTT. The simple index has actually enabled us, for the first time, to extract the summertime weather systems over an extended period of 30 years. By using the index, we have carried out the composite analyses of anomalies related to the TTT events and compared these with the known TTT structure and large-scale propagation features. Results show that the anomalies related to the canonical TTT event in our study are in good agreement with earlier studies.

The synoptic features obtained using our method confirms the robustness of the index we introduced. Based on this index, further study can be carried out to understand the climate impact on TTT variability and vice versa. From analyses using the index, it is found that TTT events are associated with a cyclonic circulation system over southern Africa and SWIO. The cyclonic circulation over southern Africa is associated with convergence of moisture, which indicates the importance of latent heat release in the maintenance of this circulation. Low level easterly anomalies of winds over the tropical southwest Indian Ocean, resulting from increased pressure gradients and the strengthening of the south Indian anticyclone, are associated with increased moisture fluxes to the adjacent continental regions of southern Africa. The passage of northeasterly flow over the oceanic region to the north of Madagascar is an important source of moisture flux over southern Africa. Easterlies to northeasterly winds around the Mascarene high in the southern Indian Ocean contribute to the poleward flow along the TTT. The mechanism for generating the TTT is associated with the strengthening of the easterly winds which results in stronger moisture fluxes toward southeast Africa.

Development of a continental low over southwest Africa enhances the low level westerly flow facilitating anomalous moisture convergence over southeast Africa. The Angola Low, a well-known feature of southern African summer circulation, plays a role in the TTT evolution and facilitates the moisture transport into subtropical southern Africa. However, the amount of moisture transported by westerlies from the eastern tropical South Atlantic Ocean to western Africa, north of the Angola Low, is relatively small. The primary moisture supply is due to northeasterlies from the Indian Ocean.

Further analysis suggests that the anomalous background condition associated with the TTT formation is linked to the La Niña-type conditions in the Pacific. The La Niña condition modifies the Walker circulation, with upper level convergence over the Indian Ocean near the African continent and Madagascar. The region of upper level convergence draws flow from all the directions, creating a region of surface divergence over the SWIO and hence encouraging low level convergence over southern Africa. The region of convergence over southern Africa is further enhanced with an interaction with upper level transients approaching the region

through the midlatitude wave-guide. These Rossby waves may, in turn, again be linked to higher than normal convection over the Sumatra region. We find that ENSO could influence the TTT genesis through the extratropical teleconnections of the southern hemisphere waveguide. Also, the ITCZ structure is seen to change over southern Africa/Madagascar prior to the TTT evolution but remains closer to climatology over other regions. Therefore, the results here indicate that the continental part of the ITCZ intensifies prior to the event and then spreads southward following the mid-latitude influence during and after the event.

Though the analysis in this study is based on strong TTT events, one can also find weak TTT events by modifying the index (reducing the standard deviation of OLR to 1.0) described in Section 4. We believe that the present study, together with the introduction of the new TTT index, provides a good opportunity to develop a predictive system, either statistical or model-based, for extreme synoptic disturbances with large socio-economic impacts in southern Africa. This study uses two variables and two equations to define the index but the method uses readily available OLR and wind data to identify the TTT systems over southern Africa. Although there are three identified domains of the TTT depending on its breeding ground, this study focuses on events that originate and are responsible for rainfall over the southern African landmass. We hope the results presented here can provide a useful framework to investigate the possible precursors. We plan to investigate these aspects further in future work using other reanalysis data and high resolution model outputs.

Acknowledgements:

This research is supported by The Japan Science and Technology Agency (JST)/Japan International Cooperation Agency (JICA) through Science and Technology Research Partnership for Sustainable Development (SATREPS). The NCEP reanalysis, interpolated OLR and the high resolution SST data were provided by NOAA/OAR/ESRL/PSD, Boulder, Colorado, USA through their web site at http://www.esrl.noaa.gov/psd. The authors thank Dr. Willem Landman and Prof. Hannes Rautenbach for their valuable suggestions. Thanks to Dr. Desmond Manatsa and Dr. Wing-Le Chan for their help in improving the manuscript. We also thank three anonymous reviewers for their constructive comments.

References

Adler RF, Huffman GJ, Chang A, Ferraro R, Xie P, Janowiak J, Rudolf B, Schneider U, Curtis S, Bolvin D, Gruber A, Susskind J, Arkin P, (2003) The Version 2 Global Precipitation Climatology Project (GPCP) Monthly Precipitation Analysis (1979-Present). J. Hydrometeor 4: 1147-1167

Behera SK, Krishnan R, Yamagata T (1999) Unusual ocean-atmosphere conditions in the tropical Indian Ocean during 1994. Geophys Res Lett 26: 3001–3004

Behera SK, Luo JJ, Masson S, Delecluse P, Gualdi S, Navarra A, Yamagata T (2005) Paramount Impact of the Indian Ocean Dipole on the East African Short Rains: A CGCM Study. J. Climate 18: 4514-4530

Behera SK, Yamagata T (2001) Subtropical SST dipole events in the southern Indian Ocean. Geophys Res Lett 28: 327–330

Behera SK., Salvekar PS, Yamagata T, 2000: Simulation of Interannual SST Variability in the Tropical Indian Ocean. J. Climate 13: 3487–3499

Chen TC (1985) Global water vapour flux and maintenance during FGGE. Mon Wea Rev 113: 1801–1819

Cook KH (2001): A Southern Hemisphere Wave Response to ENSO with Implications for Southern Africa Precipitation. *J. Atmos. Sci*, 58: 2146–2162

Cook C, Reason CJC, Hewitson BC (2004) Wet and dry spells with a particularly wet and dry summers in the South African summer rainfall region. Climate Res 26: 17–31

D'Abreton PC, Tyson PD (1995) Divergent and non-divergent water vapour transport over southern Africa during wet and dry conditions. Meteor Atmos Phys 55: 47–59

Diaz HF, Hoerling MP, Eischeid JK (2001) ENSO variability, teleconnections and climate change, Int. J. Climatol. 21: 1845–1862

Dyson LL, van Heerden J (2002) A Model for the Identification of Tropical water Systems, Water SA, 28 (3): 249-258

Fauchereau N, Pohl B, Reason C, Rouault M, Richard Y (2009) Recurrent daily OLR patterns in the southern Africa/Southwest Indian Ocean region, implications for South African rainfall and teleconnections. Climate Dyn 32: 575–591

Harrison, MSJ (1984) A generalized classification of South African summer rain-bearing synoptic systems. Int J Climatol 4: 547–560

Hart, NCG, Reason CJC, Fauchereau N (2010) Tropical–Extratropical Interactions over southern Africa: Three Cases of Heavy Summer Season Rainfall. Mon Wea Rev 138: 2608–2623

Hermes JC, Reason CJC (2009) Variability in sea-surface temperature and winds in the tropical south-east Atlantic Ocean and regional rainfall relationships. Int J Climatol 29: 11–21

Hoskins BJ, Ambrizzi Hoskins BJ (1993) Rossby wave propagation on a realistic longitudinally varying flow. J. Atmos. Sci., 50, 1661–1671.

Hoskins BJ, Karoly D (1981) The steady linear response of a spherical atmosphere to thermal and orographic forcing, J. Atmos. Sci. 38: 1179– 1196

Hsu, H.-H, Lin S.-H. (1992) Global teleconnections in the 250-mb streamfunction field during the Northern Hemisphere winter. Mon. Wea. Rev., 120, 1169–1190

Kalnay E, Kanamitsu M, Kistler R, Collins W, Deaven D, Gandin L, Iredell M, Saha S, White G, Woollen J, Zhu Y, Leetmaa A, Reynolds R, Chelliah M, Ebisuzaki W, Higgins W, Janowiak J, Mo KC, Ropelewski

C, Wang CJ, Jenne R, Joseph D (1996) The NCEP/NCAR 40-year reanalysis project. Bull Amer Meteor Soc 77: 437–471

Kidson JW, Revell MJ, Bhaskaran B, Mullan AB, Renwick JA (2002) Convection patterns in the tropical Pacific and their influence on the atmospheric circulation at high latitudes, J. Clim. 15: 137–159

Kistler, R et al. (2001), The NCEP-NCAR 50-year reanalysis: Monthly means CD-ROM and documentation, Bull. Am. Meteorol. Soc., 82, 247–268

Liebmann B, Smith CA (1996) Description of a Complete (Interpolated) Outgoing Longwave Radiation Dataset. Bull Amer Meteor Soc 77: 1275-1277

Manhique AJ, Reason CJC, Rydberg L, Fauchereau N (2011) ENSO and Indian Ocean sea surface temperatures and their relationships with tropical temperate troughs over Mozambique and the Southwest Indian Ocean. Int J Climatol 31: 1–13

Pohl B, Fauchereau N, Richard Y, Rouault M, Reason C (2009) Interactions between synoptic, intraseasonal and interannual convective variability over Southern Africa. Clim Dyn 33:1033–1050.

Racz Z, Smith RK (1999) The dynamics of heat lows. Quart J Roy Meteor Soc 125: 225–252

Reason CJC (1998) Warm and cold events in the southeast Atlantic/southwest Indian Ocean region and potential impacts on circulation and rainfall over southern Africa. Meteorol Atmos Phys 69:49–65

Reason CJC (2001) Subtropical Indian Ocean SST dipole events and southern African rainfall. Geophy Res Lett 28:2225–2227

Reason CJC, Landman W, Tennant W (2006) Seasonal to decadal prediction of southern African climate and its links with variability of the Atlantic Ocean. Bull Amer Meteor Soc 87: 941–955

Reason CJC, Mulenga H (1999) Relationships between South African rainfall and SST anomalies in the Southwest Indian Ocean. Intern J Climatol 19: 1651–1673

Reynolds RW, Smith TM, Liu C, Chelton DB, Casey KS, Schlax MG (2007) Daily high-resolution blended analyses for sea surface temperature. J Climate 20: 5473-5496

Richard Y, Trzaska S, Roucou P, Rouault M (2000) Modification of the Southern African rainfall variability/ENSO relationship since late 1960's. Clim Dyn 16: 883–895

SADC (2001) Southern African Regional Rainfall Outlook Seasonal Update No. 3., southern Africa Development Community (SADC) Drought Monitoring Center report (http://reliefweb.int/node/75822).

Saji NH, Goswami BN, Vinayachandran PN, Yamagata T (1999) A dipole mode in the tropical Indian Ocean. Nature 401: 360-363.

Todd MC, Washington R (1999) Circulation anomalies associated with tropical–temperate troughs over southern Africa and the southwest Indian Ocean. Clim Dyn 15: 937–951

Todd MC, Washington R. and Palmer PI (2004) Water vapour transport associated with tropical-temperate trough systems over southern Africa and the southwest Indian Ocean Int J Climatol 24: 555–568

Trenberth, K. E., D. P. Stepaniak, J. W. Hurrell, and M. Fiorino (2001), Quality of reanalyses in the tropics, J. Clim., 14, 1499– 1510.

Trenberth, K.E., Branstator GW, Karoly D, Kumar A, Lau NC, Ropelewski C (1998) Progress during TOGA in understanding and modeling global teleconnections associated with tropical sea surface temperatures. J. Geophys. Res. 103: 14,291–14,324

Van den Heever, SC, D'Abreton PC, Tyson PD (1997) Numerical simulation of tropical-temperate troughs over Southern Africa using the CSU RAMS model. South African Journal of Science, vol. 93 (8): 359-365

Vigaud N, Pohl B, Crétat J (2012) Tropical-temperate interactions over Southern Africa simulated by a regional climate model. Climate Dynamics, doi:10.1007/s00382-012-1314-3

Vigaud N, Richard Y, Rouault M, Fauchereau N (2009) Moisture transport between the South Atlantic Ocean and southern Africa: Relationships with summer rainfall and associated dynamics. Climate Dyn 32: 113–123

Washington R, Preston A (2006) Extreme wet years over southern Africa: Role of Indian Ocean sea surface temperatures, J. Geophys. Res. 111, D15104, doi:10.1029/2005JD006724.

Washington R, Todd MC (1999) Tropical temperate links in southern African and southwest Indian Ocean daily rainfall. Int J Climato 19: 1601–1616

Williams CJR, Kniveton DR, Layberry R (2007) Climatic and oceanic associations with daily rainfall extremes over southern Africa. Int J Climato 27: 93–108

Yamagata T, Behera SK, Luo JJ, Masson S, Jury MR, Rao SA (2004) Coupled Ocean-Atmosphere variability in the Tropical Indian Ocean, Earth's climate:The Ocean-Atmosphere Interaction Geophysical Monograph Series 147, Eds. by Wang, C., S.-P. Xie, and J.A. Carton., 2004.

Figure captions:

Figure 1: December-January-February (DJF) climatology of (a) outgoing longwave radiation (Wm^{-2}), (b) sea level pressure (shaded, hPa) and surface temperature (contour, degree C), (c) 850 hPa geopotential height (shaded, m) and winds (vector, m/s), (d) same as (c) but for 500 hPa, (e) 850 hPa divergence (shaded, $*e^{-5}/s$) and vertical velocity (contour, Pa/s) and (f) same as (e) but for 500 hPa.

Figure 2: Various regions chosen for identifying the index. Filled rectangle boxes (E1, E2, W1 and W2) are used for OLR and dashed rectangular boxes (W and E) are used for wind.

Figure 2 (b): Composite structure of OLR and wind for 91 TTT events and (c) same as (b) but for 198 TTT events derived using the index.

Figure 3: Annual frequency of TTTs for the period 1980-2009. The red line indicates the mean frequency of TTT events.

Figure 4: Standardized anomaly of OLR and winds for the 55 TTT events during the period 1980-2009 (The anomalies for remaining days are suppressed for the clarity of those 55 events).

Figure 5: Composites anomaly of outgoing longwave radiation (Wm^{-2} , significant at the 90 % level using a student's t-test).

Figure 6: Composite anomalies of 200 hPa velocity potential (shaded). Values are significant at the 90% level using a student's t-test and the units are $1x10^6$ m^2 s^{-1}. Divergent component of the winds (vectors, units: m^{-1} s^{-1}) are overlaid.

Figure 7: Composite anomalies of 850 hPa velocity potential (shaded). Values are significant at the 90% level using a student's t-test and the units are $1x10^6$ m^2 s^{-1}. Divergent component of the winds (vectors, units: m^{-1} s^{-1}) are overlaid.

Figure 8: Composites anomalies of sea surface temperature (K). Shown values are significant at the 90 % level using a student's t-test.

Figure 9: Composites anomalies of OLR (Wm^{-2}, shown values are significant at 95 % using a student's t-test) and wind vectors (thick arrows are significant at the 90 % level using a student's t-test).

Figure 10: Composites anomalies of sea level pressure (hPa, Shaded values are significant at the 95 % level using a student's t-test).

Figure 11: Composites anomalies of 850 hPa Omega (Pa/s) (Shaded values are significant at the 95 % level using a student's t-test).

Figure 12: Composite anomalies of 850 hPa streamfunction (shaded, significant at the 95 % level using t-test are contoured, units: $1x10^6$ m^2 s^{-1}) and rotational component of moisture transport (units: gm m^{-1} s^{-1}).

Figure 13: Composite anomalies of 850 hPa velocity potential (shaded, significant at the 95 % level using t-test is contoured units: $1x10^6$ m^2 s^{-1}) and divergent component of moisture transport (vectors, units: gm m^{-1} s^{-1}).

Figure 14: Composite anomalies of 200 hPa meridional winds (m/s, shown values are significant at the 90 % level using a student's t-test).

Figure 15: Composites of outgoing longwave radiation (Wm^{-2}).

Figure.16: DJF composite anomalies of rainfall (mm/day) [a, b], sea surface temperature (K, shaded) and 200 hPa velocity potential ($10^6m^2s^{-1}$, contour) [c, d], 200 hPa geopotential height (m, shaded) and meridional wind (contour, 0.5, 1, 2 and 3 m/s) [e, f] for El Niño and La Niña seasons during the 30 year period used in our study.

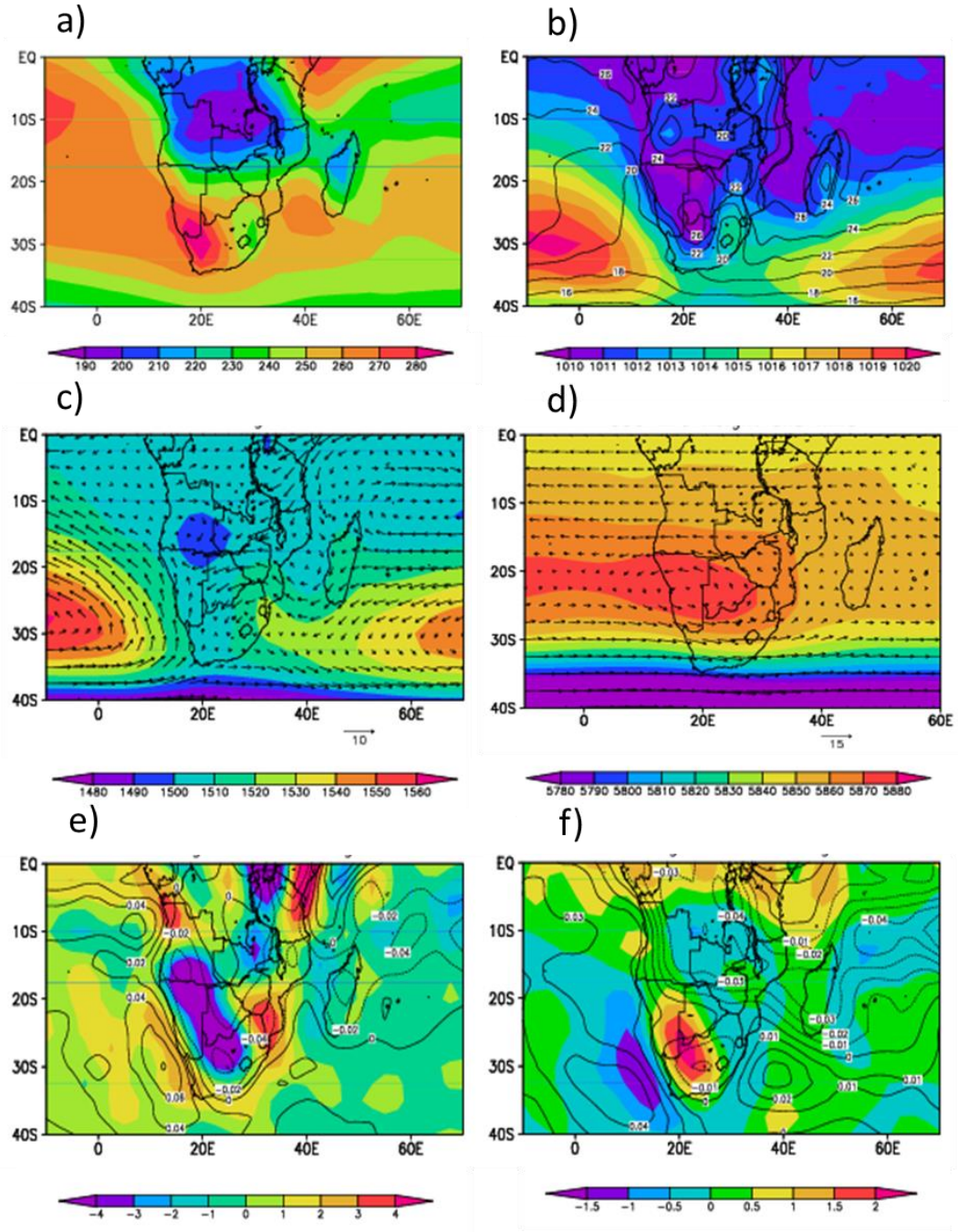

Figure 1: December-January-February (DJF) climatology of (a) outgoing longwave radiation (Wm^{-2}), (b) sea level pressure (shaded, hPa) and surface temperature (contour, degree C), (c) 850 hPa geopotential height (shaded, m) and winds (vector, m/s), (d) same as (c) but for 500 hPa, (e) 850 hPa divergence (shaded, *e-5/s) and vertical velocity (contour, Pa/s) and (f) same as (e) but for 500 hPa.

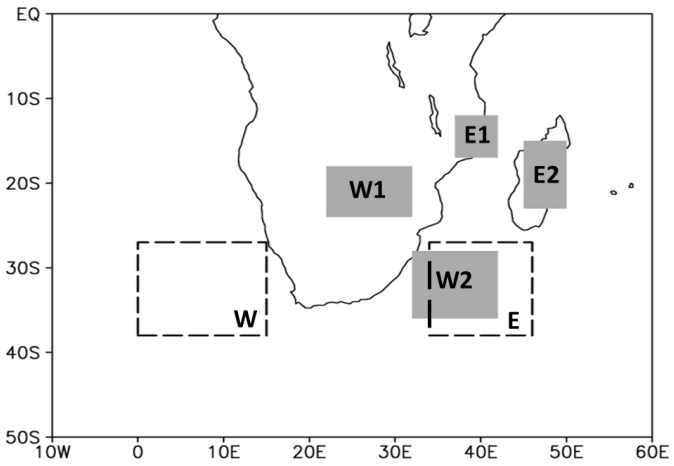

Figure 2 (a): Various regions chosen for identifying the index. Filled rectangle boxes (E1, E2, W1 and W2) are used for OLR and dashed rectangular boxes (W and E) are used for wind.

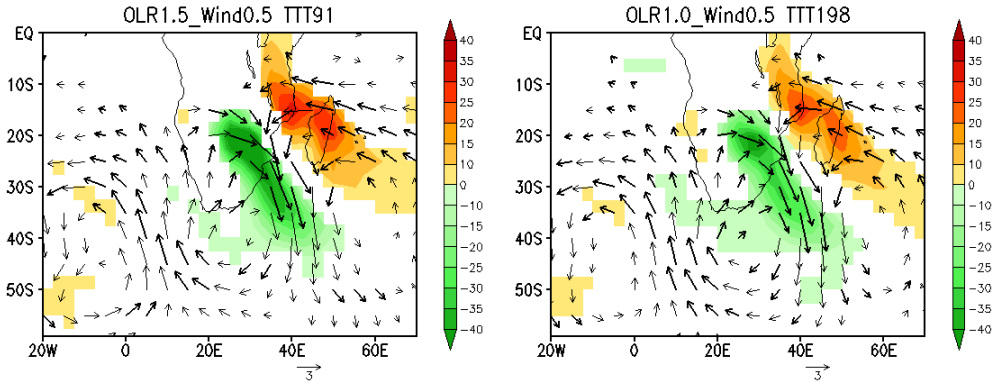

Figure 2 (b): Composite structure of OLR and wind for 91 TTT events and (c) same as (b) but for 198 TTT events derived using the index.

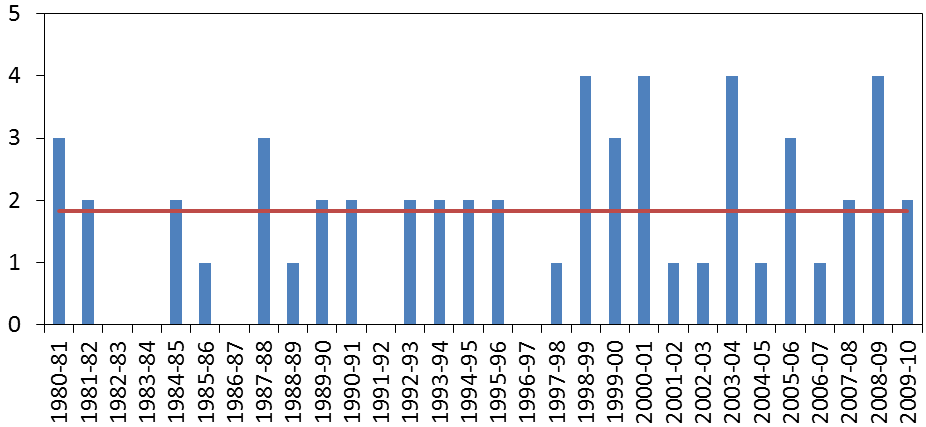

Figure 3: Annual frequency of TTTs for the period 1980-2009. The red line indicates the mean frequency of TTT events.

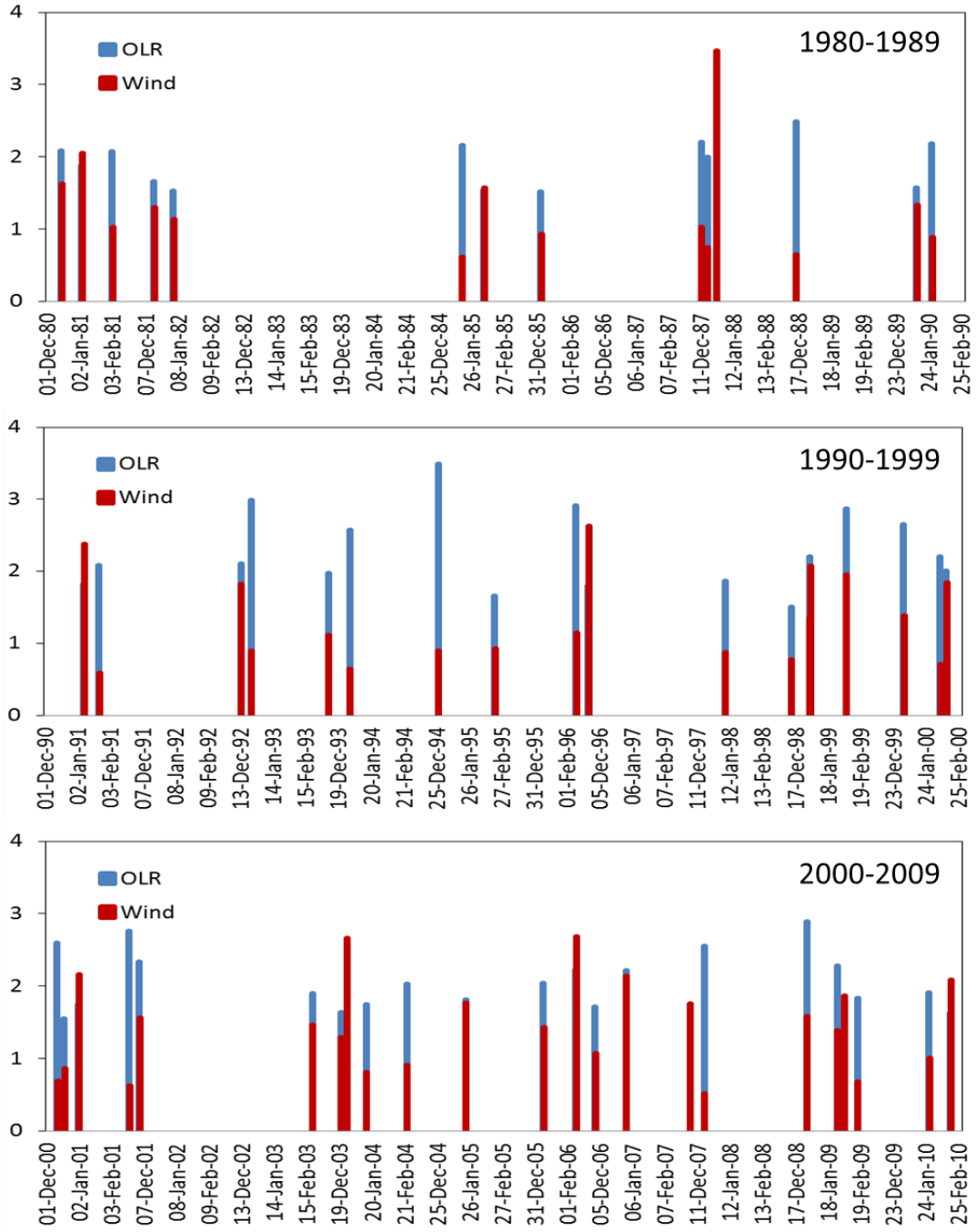

Figure 4: Standardized anomaly of OLR and winds for the 55 TTT events during the period 1980-2009 (The anomalies for remaining days are suppressed for the clarity of those 55 events).

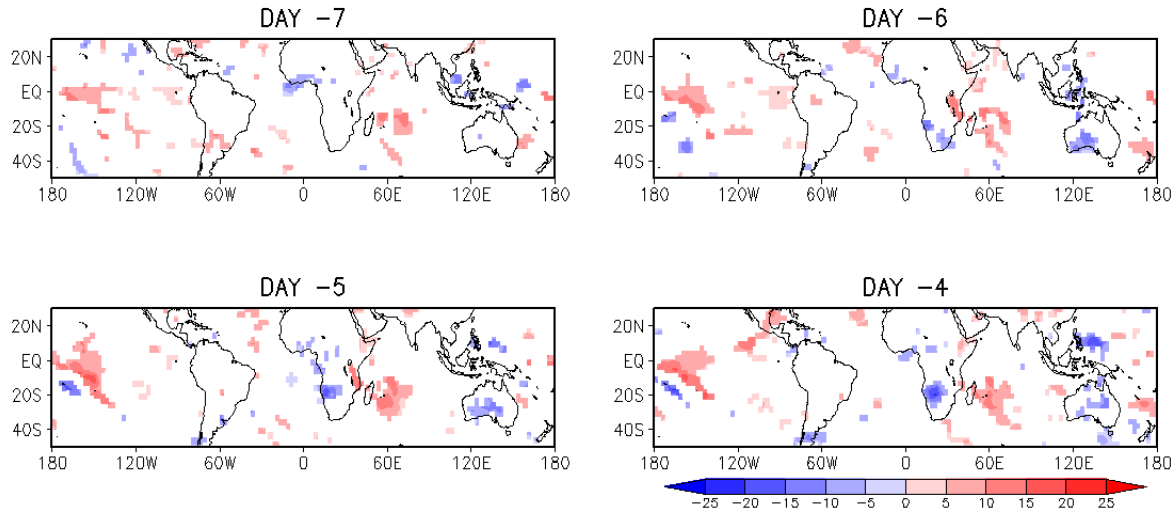

Figure 5: Composites anomaly of outgoing longwave radiation (Wm^{-2}, shown values are significant at the 90 % level using a student's t-test).

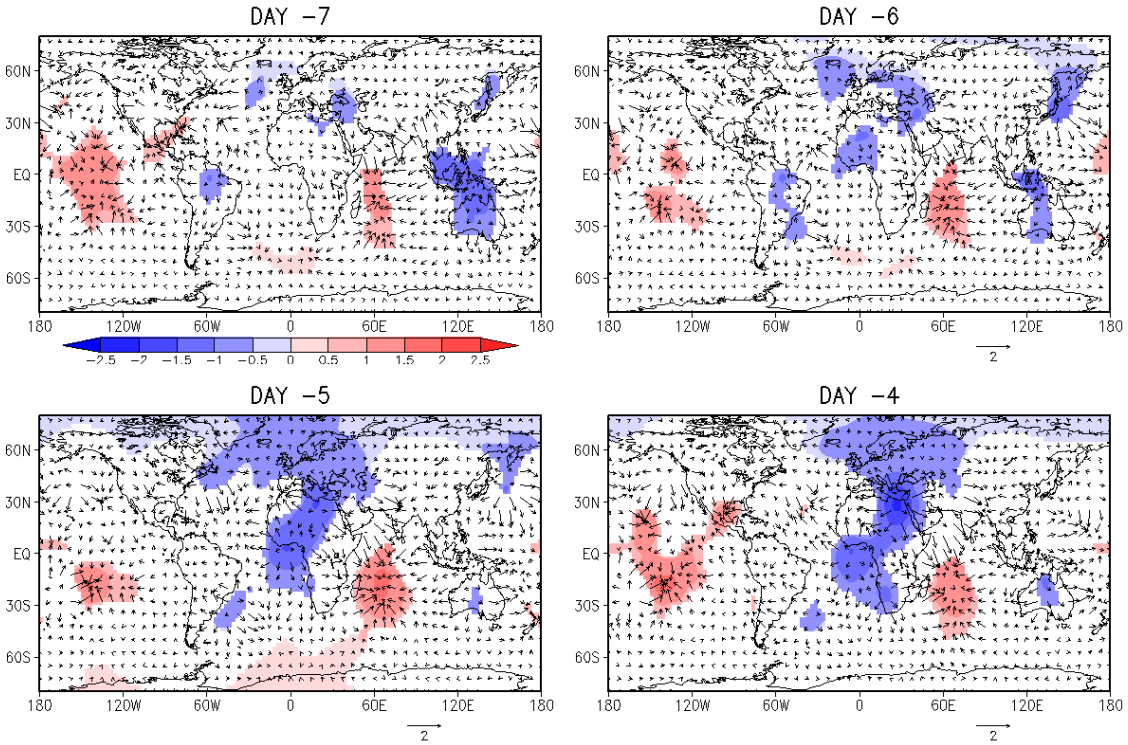

Figure 6: Composite anomalies of 200 hPa velocity potential (shaded). Values are significant at the 90% level using a student's t-test and the units are $1x10^6$ m^2 s^{-1}. Divergent component of the winds (vectors, units: m^{-1} s^{-1}) are overlaid.

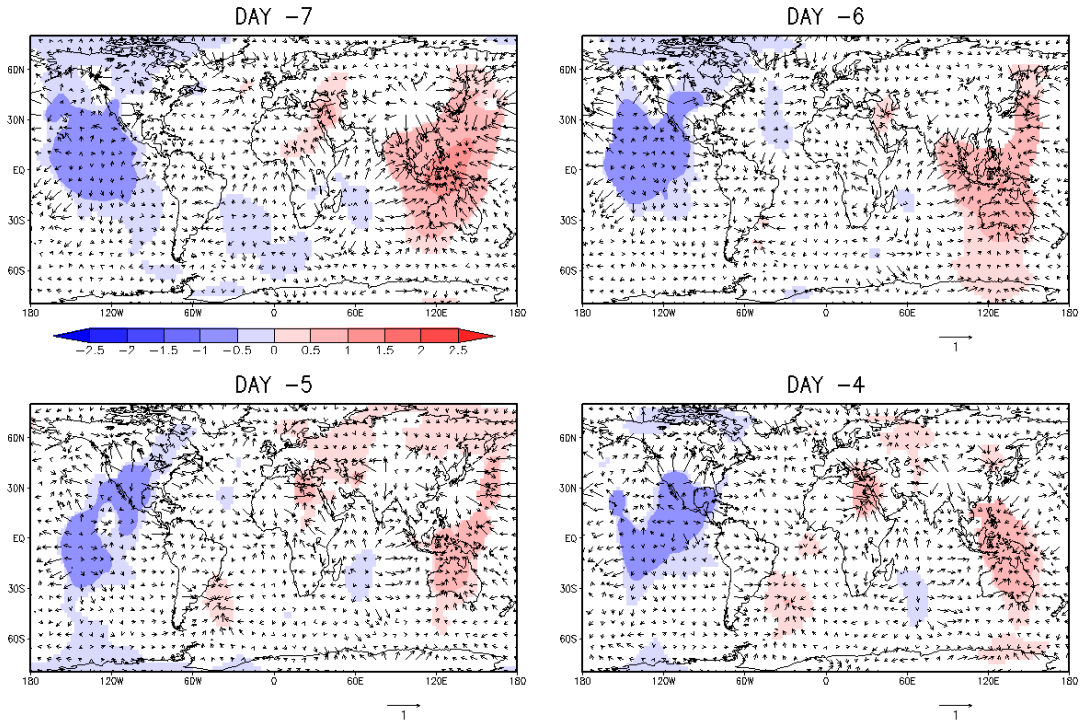

Figure 7: Composite anomalies of 850 hPa velocity potential (shaded). Values are significant at the 90% level using a student's t-test and the units are $1x10^6$ m^2 s^{-1}. Divergent component of the winds (vectors, units: m^{-1} s^{-1}) are overlaid.

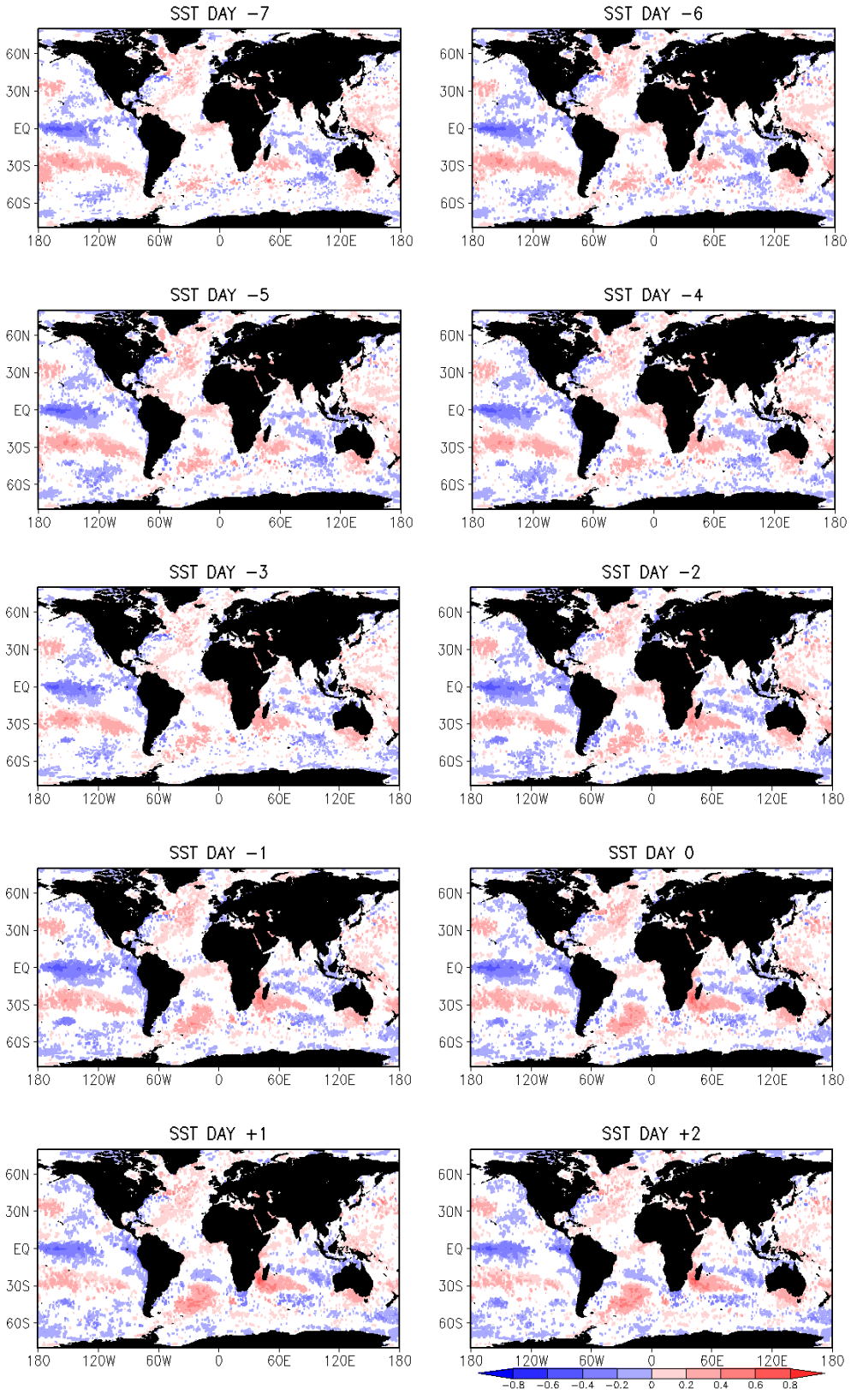

Figure 8: Composites anomalies of sea surface temperature (K). Shown values are significant at the 90 % level using a student's t-test.

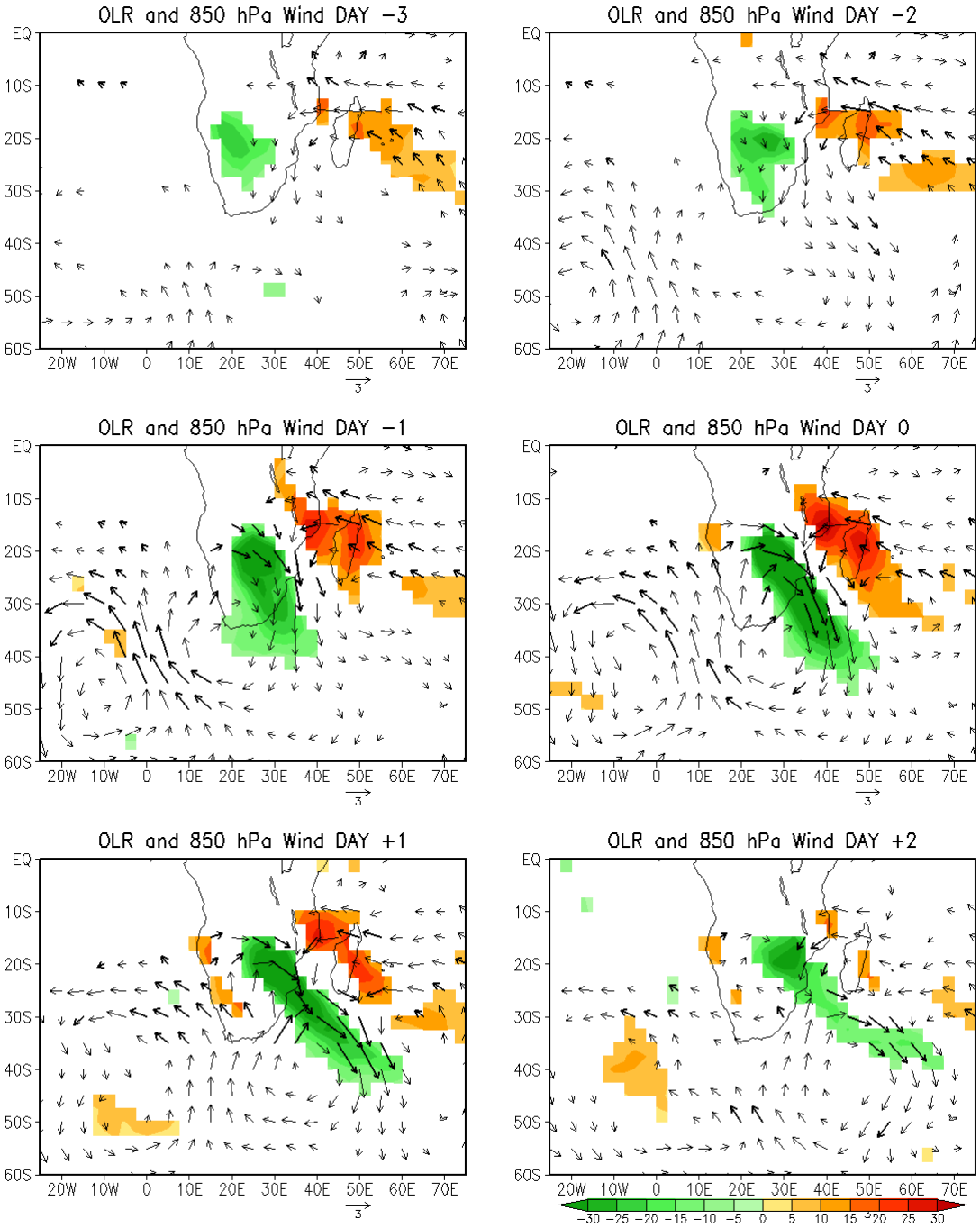

Figure 9: Composites anomalies of OLR (Wm^{-2}, shown values are significant at the 95 % level using a student's t-test) and wind vectors (thick arrows are significant at the 90 % level using a student's t-test).

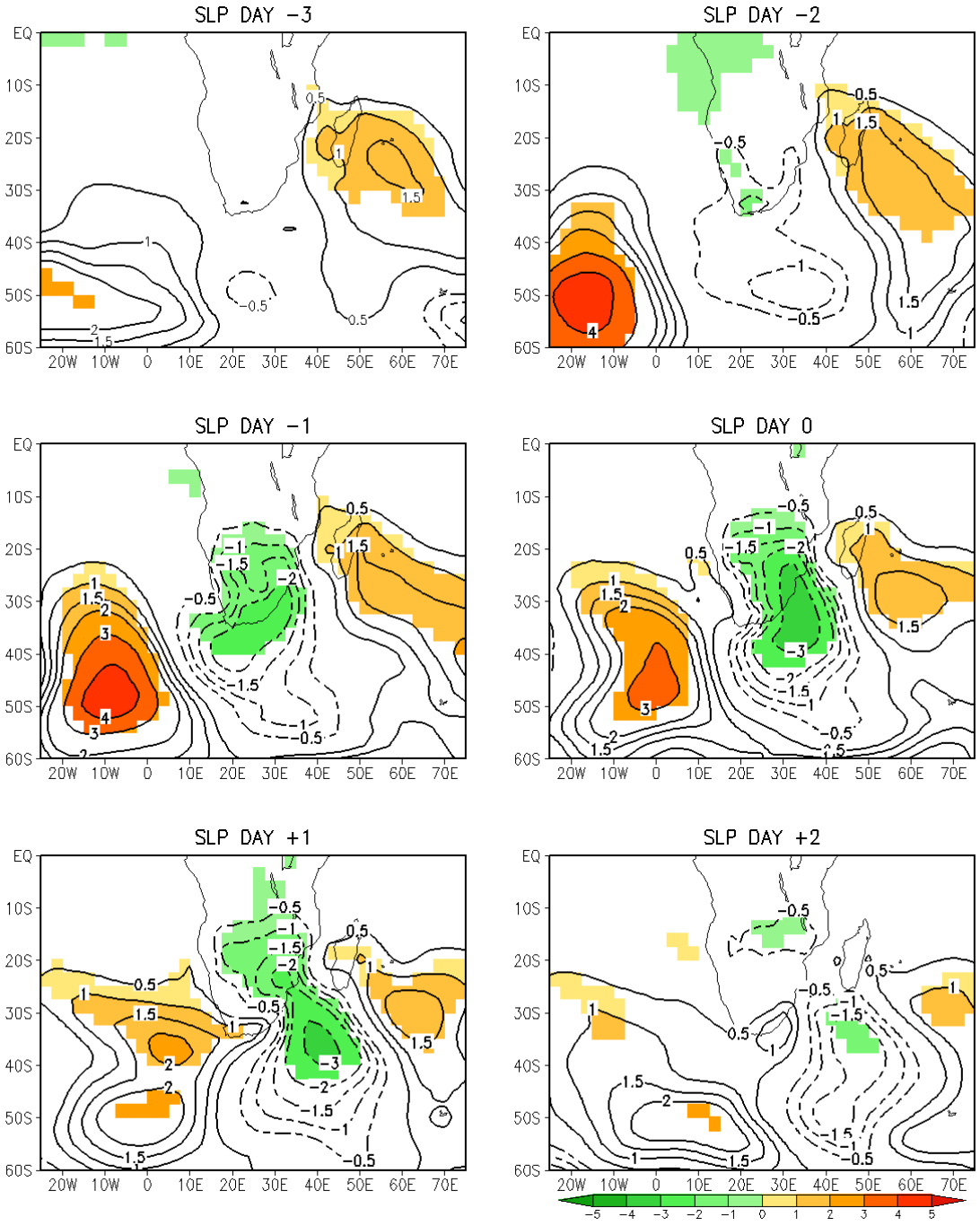

Figure 10: Composites anomalies of sea level pressure (hPa, Shaded values are significant at the 95 % level using a student's t-test).

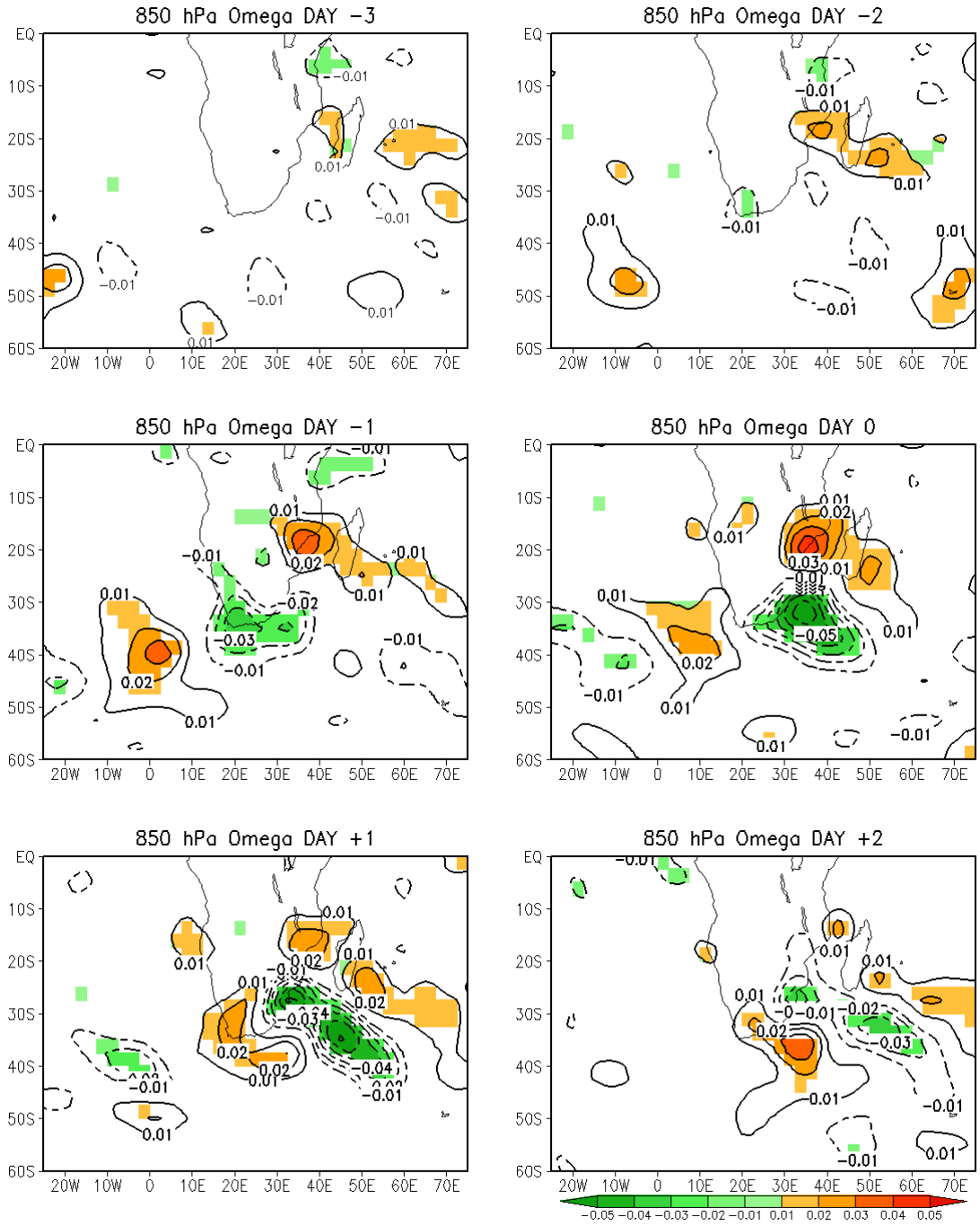

Figure 11: Composites anomalies of 850 hPa Omega (Pa/s, Shaded values are significant at the 95 % level using a student's t-test).

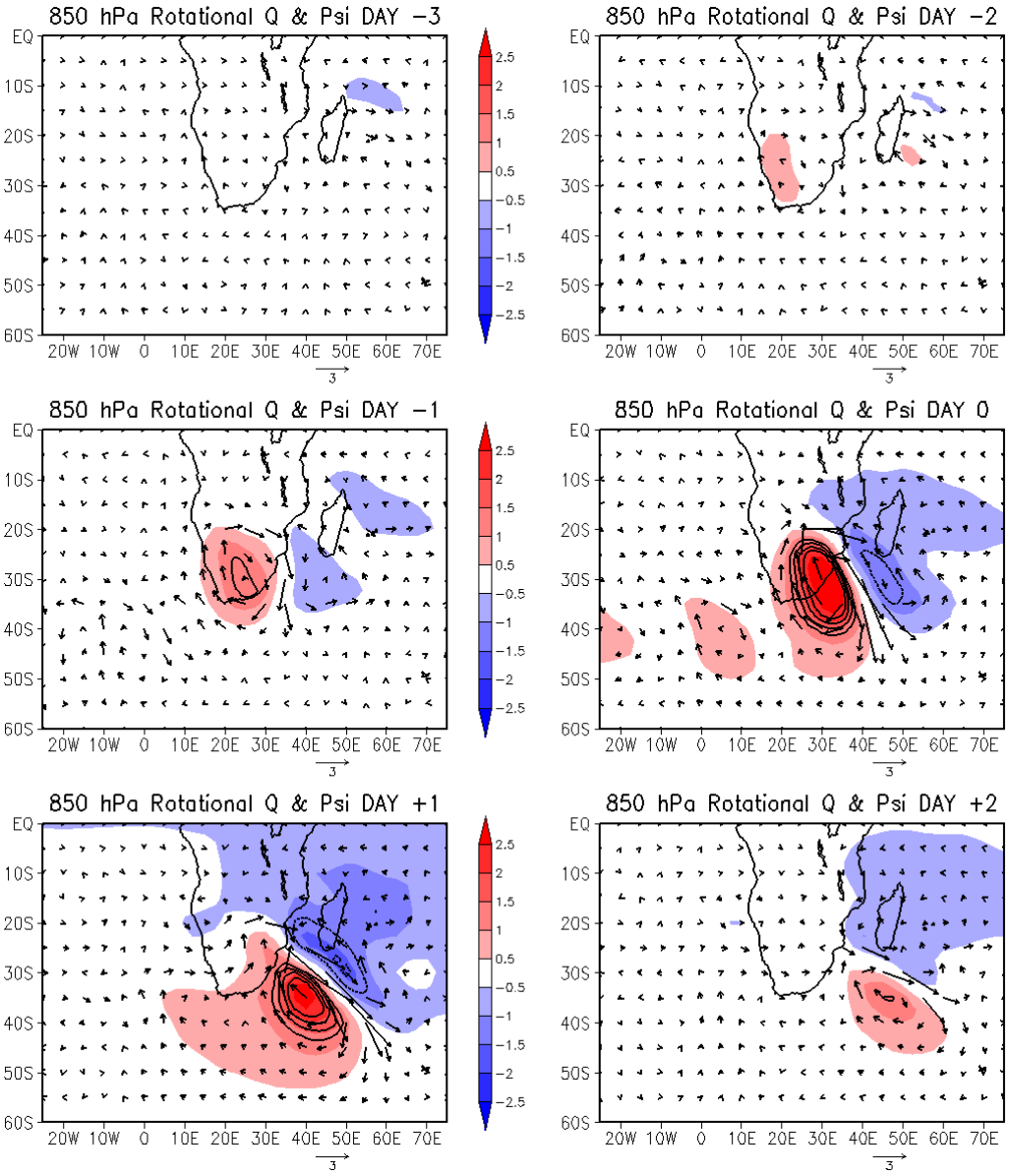

Figure 12: Composite anomalies of 850 hPa streamfunction (shaded, significant at the 95 % level using t-test are contoured, units: $1x10^6$ m^2 s^{-1}) and rotational component of moisture transport (units: gm m^{-1} s^{-1}).

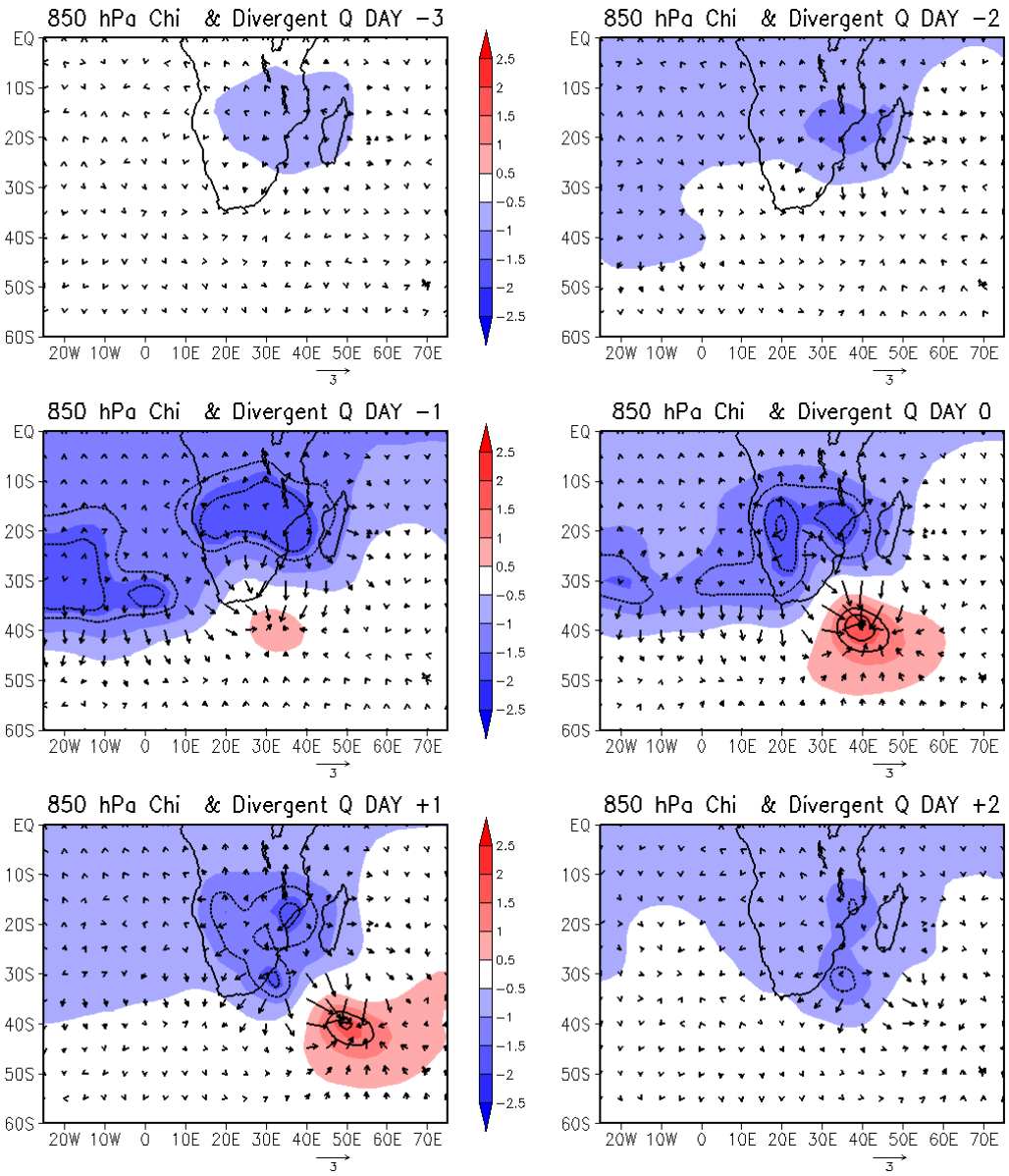

Figure 13: Composite anomalies of 850 hPa velocity potential (shaded, significant at the 95 % level using t-test is contoured units: $1x10^6$ m^2 s^{-1}) and divergent component of moisture transport (vectors, units: gm m^{-1} s^{-1}).

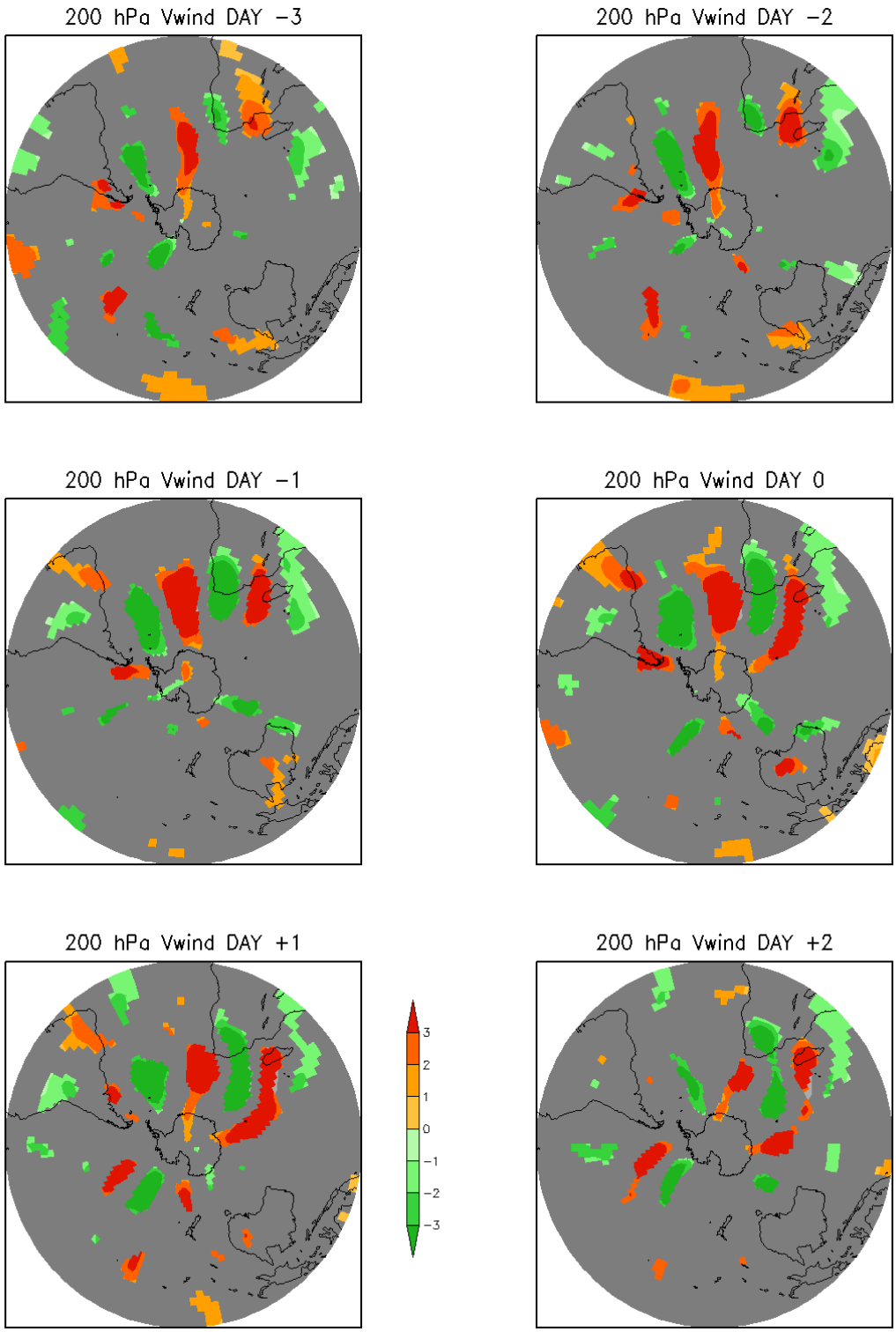

1
2
3 Figure 14: Composite anomalies of 200 hPa meridional wind (m/s, Shown values are significant at the
4 90 % level using a student's t-test).

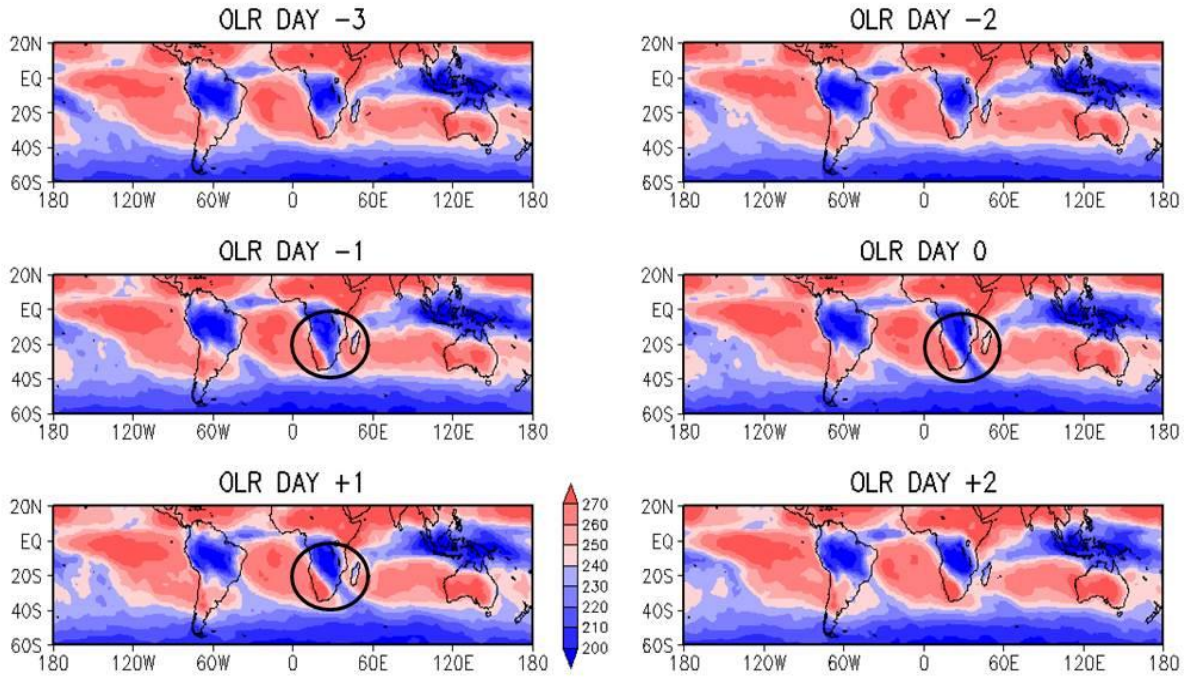

Figure 15: Composites of outgoing longwave radiation (Wm^{-2}) during the TTT events.

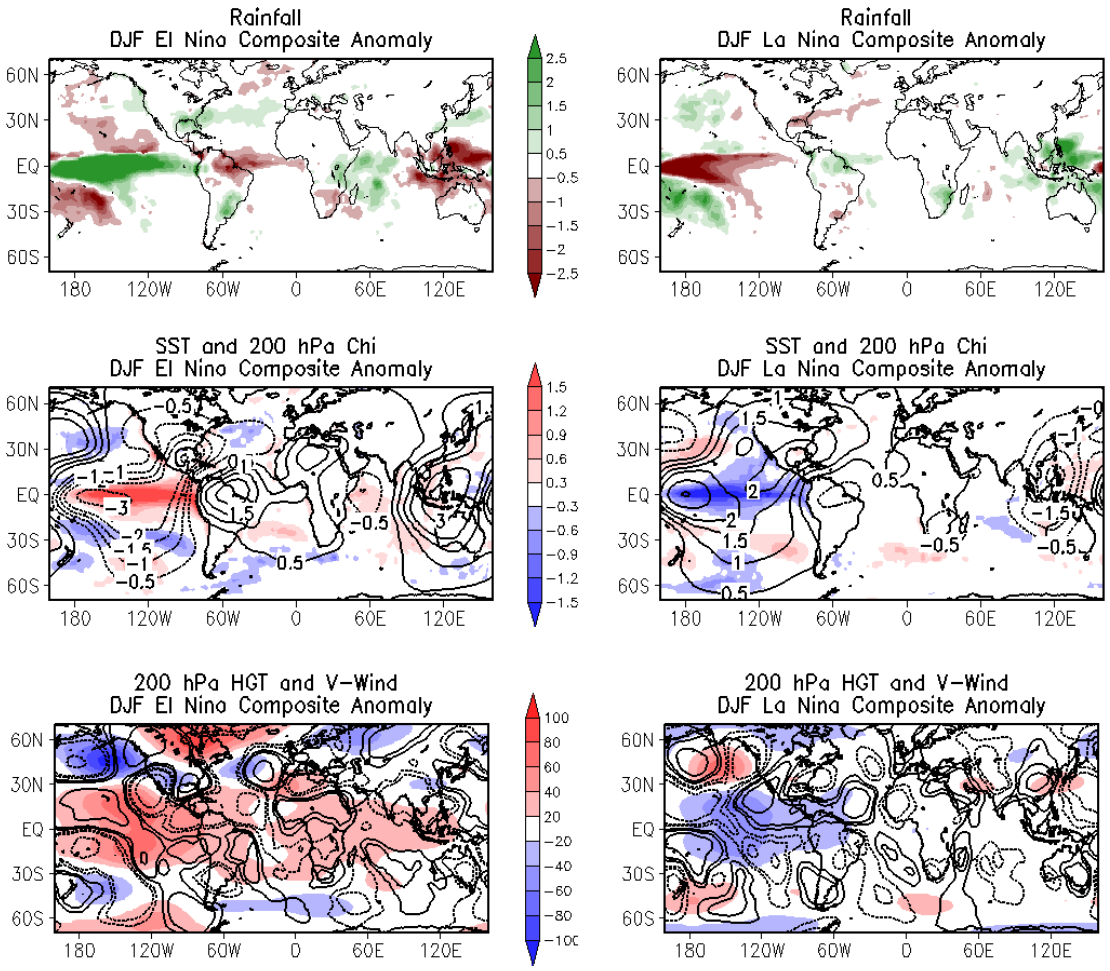

Fig.16: DJF composite anomalies of rainfall (mm/day) [a, b], sea surface temperature (K, shaded) and 200 hPa velocity potential ($10^6 m^2 s^{-1}$, contour) [c, d], 200 hPa geopotential height (m, shaded) and meridional wind (contour, 0.5, 1, 2 and 3 m/s) [e, f] for El Niño and La Niña seasons during the 30 year period used in our study.